

## Article

# Economic Dispatch Model of High Proportional New Energy Grid-Connected Consumption Considering Source Load Uncertainty

Min Xu <sup>1</sup>, Wanwei Li <sup>1</sup>, Zhihui Feng <sup>1</sup>, Wangwang Bai <sup>1</sup>, Lingling Jia <sup>2,3</sup> and Zhanhong Wei <sup>2,\*</sup> <sup>1</sup> Economic Technology Research Institute of State Grid Gansu Electric Power Company, Lanzhou 730050, China<sup>2</sup> College of Electrical and Information Engineering, Lanzhou University of Technology, Lanzhou 730050, China<sup>3</sup> Shenzhen Zhongdian Electric Power Technology Co., Ltd., Shenzhen 518000, China

\* Correspondence: eezhw@lut.edu.cn

**Abstract:** To solve the problem regarding the large-scale grid-connected consumption of a high proportion of new energy sources, a concentrating solar power (CSP)-photovoltaic (PV)-wind power day-ahead and intraday-coordinated optimal dispatching method considering source load uncertainty is proposed. First, the uncertainty of day-ahead wind power output prediction is described by the multi-scenario stochastic planning method, and the uncertainty of intraday source-load is characterized by the trapezoidal fuzzy number equivalence model. Second, based on the combined scenario set of day-ahead wind power output prediction, the day-ahead optimal dispatch is performed by combining thermal and CSP plants, and the day-ahead thermal and CSP plant dispatch output and intraday source load fuzzy dataset are used as the input quantities for the day-ahead dispatch. Thus, the scheduling output and rotating backup plan for thermal power and CSP plants were determined; finally, the validity and feasibility of the model were verified using arithmetic examples.

**Keywords:** new energy consumption; multiple time scale; uncertainty; two-level optimal



**Citation:** Xu, M.; Li, W.; Feng, Z.; Bai, W.; Jia, L.; Wei, Z. Economic Dispatch Model of High Proportional New Energy Grid-Connected Consumption Considering Source Load Uncertainty. *Energies* **2023**, *16*, 1696. <https://doi.org/10.3390/en16041696>

Academic Editor: Nicu Bizon

Received: 1 November 2022

Revised: 1 February 2023

Accepted: 6 February 2023

Published: 8 February 2023



**Copyright:** © 2023 by the authors. Licensee MDPI, Basel, Switzerland. This article is an open access article distributed under the terms and conditions of the Creative Commons Attribution (CC BY) license (<https://creativecommons.org/licenses/by/4.0/>).

## 1. Introduction

Due to the volatility and intermittency of new energy sources, large-scale grid connections lead to an increase in peak output power fluctuation. Therefore, considerable flexibility is required to adjust the power supply for peak regulation. In the new energy base, the proposed method is an effective way to ensure green and efficient consumption of new energy by making rational use of regional wind and solar energy resources, thus improving the supply of new energy such as wind power, photovoltaic (PV) and concentrating solar power (CSP) generation, and accelerating the construction of a diversified and complementary new energy supply system.

In recent years, scholars at home and abroad have made some research achievements on the uncertainty of both sides of the source load. In reference [1], a robust, fuzzy, multi-objective dispatching model of a power system was established that takes into account the source load bilateral uncertainty. In reference [2], a cross regional day-ahead and intraday scheduling model that considers the uncertainty of new energy forecasts is established through the use of a stochastic optimization model and multi-time-scale rolling optimization. In reference [3], taking into account the characteristics of load uncertainty and wind power uncertainty on the power system with a high energy load and wind power coordinated dispatching, a robust unit combination model that minimizes the risk of wind curtailment and load slitting was constructed. Reference [4] characterized the uncertainty of new energy output using the coupled quantile point regression theory and the reduced dimensional clustering technique for the generation of a new energy-combined output scenario set. Reference [5] considered the variations in wind power and load forecasting

deviation with time scale and the load response deviation under the condition of time-sharing tariff price. Reference [6] used Monte Carlo simulations to generate scenarios with different price demand responses and employed opportunity constraint methods to model expectations. Reference [7] considered the uncertainty of wind power and price-elastic demand curves and established a multilevel optimal dispatching model considering the bilateral uncertainty of the source load. In reference [8], the stochastic response characteristic of price-elastic load was used to smooth out the stochastic fluctuation characteristic of wind power. In reference [9], an uncertainty load model considering load self-elasticity coefficients and tariff-based demand response was proposed. Reference [10] established a stochastic fuzzy uncertainty model of wind farm output based on the uncertainty planning theory and expressed the uncertainty characteristics of load forecasting in terms of load interval curves. Reference [11] used fuzzy parameters to describe the uncertainty of new energy output and load demand in the system. Reference [12] used fuzzy parameters to represent intermittent power output and load uncertainty. In reference [13], a combination of goal programming based on fuzzy random chance constraints and priority goal programming was proposed to solve the dual uncertainty of user response behavior under wind power and time-sharing tariff prices. Reference [14] proposed a system risk assessment considering multiple uncertainties by integrating stochastic fuzzy characteristics such as load. To reduce the impact of PV and load output forecast uncertainty on the economy of interprovincial optimal dispatching operations, Reference [15] proposed a two-level dispatching strategy for DC interprovincial interconnected power grids considering PV load forecast uncertainty. In Reference [16], wind power and load were represented by fuzzy parameters to change the deterministic system constraints into fuzzy chance constraints based on the plausibility theory. In summary, references [1–4] improved the accuracy of the predicted new energy output through different forecasting methods, with the main purpose of alleviating the uncertainty of the new energy output. References [5–9] introduced demand response resources into system dispatching and investigated the impact of uncertainty on system load under various types of demand response regulation to learn more about its inherent uncertainty problem. In references [10–18], the uncertainty of wind power output and load demand was expressed by deterministic scenarios and fuzzy parameters, with the uncertain variables transformed into deterministic variables. However, the following problems still need to be considered: (1) most of the research on optimal dispatch of high proportion of new energy focuses on the long time scale ahead of the day, without considering the uncertainty of the short time scale within the day; (2) the use of the CSP plant with heat storage system to coordinate and optimize the uncertainty of wind and solar output is seldom considered.

This paper considers the output complementary characteristics between wind power and PV and CSP plants, as well as the dual uncertainties of high proportional power sources and loads. In addition, considering that the output prediction of renewable energy such as wind and solar energy is closely related to the time scale, when the time scale is shorter and closer to the current time, the prediction accuracy is higher. If different dispatching plans are formulated under different time scales based on the response time of various adjustable resources in the power system, the accuracy of dispatching results can be improved and the system's ability to absorb renewable energy with large fluctuations can be effectively improved. Compared with the day-ahead long-time scale, the Intraday short-time scale can be combined with more accurate intra-day prediction information and make full use of the fast adjustment ability and power translation characteristics of the CSP plant to effectively reduce the load fluctuation after the wind–solar grid connection. In addition, this paper also considers the prediction error of wind power, PV power and load demand, and establishes different source-load uncertainty models for day-ahead and intraday scheduling. The day-ahead scheduling is characterized by deterministic scenario analysis, and the intraday scheduling is based on the fuzzy parameters of wind power and load demand by introducing fuzzy theory and using trapezoidal functions to establish a two-level day-ahead and intraday scheduling model that considers the source-

load uncertainty. The simulation results verify the validity and feasibility of the model and method in this paper. This paper aims to propose a feasible scheme for the current dilemma of power system peak regulation, which requires a certain reference value to allow a CSP plant to participate in power market dispatching.

The remainder of this paper is structured as follows: Section 2 models the uncertainty of source-load, and Section 3 builds the scheduling model for the day-ahead and day-in time scales, respectively, to explain the solution methods for the models. Section 4 summarizes our case study data and results, and Section 5 comprises the conclusion.

## 2. Source Load Uncertainty Model

When establishing a scheduling model, it is very important to consider the system uncertainty. The uncertainty of day-ahead wind power and PV output is expressed by the sum of the deterministic forecast value and the changing forecast error, and the normal distribution is used to analyze the forecast error of new energy output. The uncertainty of intraday source load is described by introducing trapezoidal fuzzy parameters.

### 2.1. Uncertainty Expression of the Output of the Day Ahead

Compared with the uncertainty of wind power and PV output, the system load demand fluctuates less under the 24-h day-ahead time scale and is relatively stable, so its uncertainty will not be considered for the time being. The uncertainty of wind power and PV output is the problem to focus on in the day-ahead dispatch, and the wind power and PV output are expressed as the sum of the determined forecast value and the variable forecast error, and can be described by the following equation:

$$\begin{cases} P_{w,t} = P_{w,t,y} + P_{w,t,c} \\ P_{v,t} = P_{v,t,y} + P_{v,t,c} \end{cases} \quad (1)$$

where  $P_{w,t}$  and  $P_{v,t}$  are the output of wind power and PV, respectively;  $P_{w,t,y}$ ,  $P_{v,t,y}$ ,  $P_{w,t,c}$  and  $P_{v,t,c}$  are the constant output prediction and the variable output prediction errors of wind power and PV, respectively.

For large-scale wind farm and PV power plant output prediction problems, the normal distribution is usually used to analyze the prediction error of new energy sources. Its prediction error probability density function is as follows:

$$\begin{cases} f(P_{w,t,c}) = \frac{1}{\sqrt{2\pi}\delta_{w,t,c}} e^{-\frac{(P_{w,t,c}-\mu_{w,t,c})^2}{2\delta_{w,t,c}^2}} \\ f(P_{v,t,c}) = \frac{1}{\sqrt{2\pi}\delta_{v,t,c}} e^{-\frac{(P_{v,t,c}-\mu_{v,t,c})^2}{2\delta_{v,t,c}^2}} \end{cases} \quad (2)$$

where  $\delta_{w,t,c}$ ,  $\delta_{v,t,c}$ ,  $\mu_{w,t,c}$  and  $\mu_{v,t,c}$  are the variance and expectation values of wind power and PV prediction errors at time  $t$ , respectively.

### 2.2. Intraday Trapezoidal Fuzzy Number Equivalence Model

#### 2.2.1. Trapezoidal Fuzzy Number Expression

Let  $\tilde{a}$  be a fuzzy number if the membership function of  $\tilde{a}$  is:

$$s_{\tilde{a}}(x) = \begin{cases} \frac{\omega(x-u_1)}{u_2-u_1} & u_1 \leq x \leq u_2 \\ \omega & u_2 \leq x \leq u_3 \\ \frac{\omega(u_4-x)}{u_4-u_3} & u_3 \leq x \leq u_4 \\ 0 & \text{other} \end{cases} \quad (3)$$

where  $u_1$ ,  $u_2$ ,  $u_3$  and  $u_4$  are called trapezoidal fuzzy number membership parameters,  $u_1 \leq u_2 \leq u_3 \leq u_4$ , and  $u_i \in R(i = 1, 2, 3, 4)$ ; Call  $\tilde{a}$  the trapezoidal fuzzy number and

denote it as  $\tilde{a} = (u_1, u_2, u_3, u_4, \omega)$ .  $S_{\tilde{a}}(x)$  is the membership function and  $S_{\tilde{a}}(x) \in [0, 1]$ . Call  $[u_1, u_4]$  the support interval of the fuzzy number  $\tilde{a}$  and call  $[u_2, u_3]$  the peak interval of the fuzzy number  $\tilde{a}$ .  $0 \leq \omega \leq 1$  is a constant, and when  $\omega = 1$ ,  $u = (u_1, u_2, u_3, u_4, \omega)$  is the regular trapezoidal fuzzy number, denoted as  $u = (u_1, u_2, u_3, u_4)$ ; then:

$$s_{\tilde{a}}(x) = \begin{cases} \frac{x-u_1}{u_2-u_1} & u_1 \leq x \leq u_2 \\ 1 & u_2 \leq x \leq u_3 \\ \frac{u_4-x}{u_4-u_3} & u_3 \leq x \leq u_4 \\ 0 & \text{other} \end{cases} \tag{4}$$

The trapezoidal fuzzy parameter  $\tilde{P}$  can be represented by the quaternion trapezoidal fuzzy parameter  $\tilde{P}$  and can be represented by four tuples, which can be expressed as:

$$\tilde{P} = (u_1, u_2, u_3, u_4) = (k_1, k_2, k_3, k_4)P^f \tag{5}$$

where  $k_1, k_2, k_3$  and  $k_4$  are proportional coefficients;  $\tilde{P}$  is the fuzzy representation of  $P$  and  $P^f$  is the predicted value of  $P$ .

The trapezoidal fuzzy parameter diagram is shown in Figure 1.

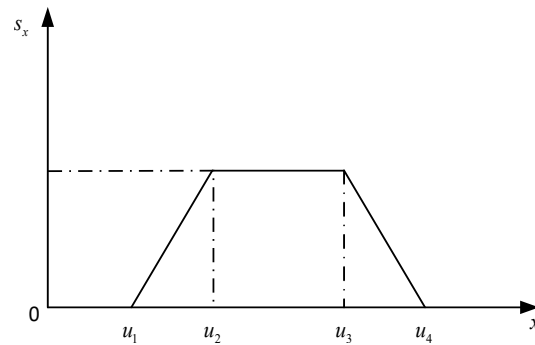


Figure 1. Trapezoidal fuzzy parameter diagram.

### 2.2.2. Uncertainty Expression of Wind, PV and Load

In intraday optimal scheduling, regular trapezoidal fuzzy numbers are used to characterize the uncertainty problem of wind PV and load. The wind power, PV and load are represented by quadratic sets of trapezoidal fuzzy parameters  $\tilde{P}_{w,t}$ ,  $\tilde{P}_{v,t}$  and  $\tilde{P}_{l,t}$  as follows:

$$\begin{cases} \tilde{P}_{w,t} = (P_{w1,t}, P_{w2,t}, P_{w3,t}, P_{w4,t}) \\ \tilde{P}_{v,t} = (P_{v1,t}, P_{v2,t}, P_{v3,t}, P_{v4,t}) \\ \tilde{P}_{l,t} = (P_{l1,t}, P_{l2,t}, P_{l3,t}, P_{l4,t}) \end{cases} \tag{6}$$

where  $P_{wi,t}$ ,  $P_{vi,t}$  and  $P_{li,t}$  are the corresponding trapezoidal membership parameters.

$$\begin{cases} P_{wi,t} = k_{wi} * P_{w\_t}^f \\ P_{vi,t} = k_{vi} * P_{v\_t}^f \\ P_{li,t} = k_{li} * P_{l\_t}^f \end{cases} \tag{7}$$

Then, the specific formulas for describing wind power, PV, and load through fuzzy parameters are as follows:

$$\begin{cases} \tilde{P}_{w,t} = (k_{w1}P_{w\_t}^f, k_{w2}P_{w\_t}^f, k_{w3}P_{w\_t}^f, k_{w4}P_{w\_t}^f) \\ \tilde{P}_{v,t} = (k_{v1}P_{v\_t}^f, k_{v2}P_{v\_t}^f, k_{v3}P_{v\_t}^f, k_{v4}P_{v\_t}^f) \\ \tilde{P}_{l,t} = (k_{l1}P_{l\_t}^f, k_{l2}P_{l\_t}^f, k_{l3}P_{l\_t}^f, k_{l4}P_{l\_t}^f) \end{cases} \tag{8}$$

where  $P_{w,t}^f$ ,  $P_{v,t}^f$  and  $P_{l,t}^f$  are the predicted values of wind power and PV output and load, respectively;  $k_{wi}$ ,  $k_{vi}$  and  $k_{li}$  are proportional coefficients, and  $i = 1, 2, 3, 4$ .

### 3. Scheduling Model of Each Time Scale

The upper layer of the scheduling model takes the minimum expected value of the system residual load variance as the optimization goal, and the lower layer takes the lowest total operating cost of the thermal power units and CSP plant as the optimization goal, while also considering the power balance constraints, unit output constraints, unit rotating reserve constraints, ramp rate constraints, thermal storage system constraints to establish a scheduling model for each time scale. The commercial optimization software CPLEX is called through YALMIP to solve the problem.

#### 3.1. Day-Ahead Scheduling Plan Model

##### (1) Objective function

The 24-h day-ahead dispatching of the day is divided into two layers. The upper model takes the minimum expected value of the system residual load variance as the objective function as follows:

$$\begin{cases} f_1 = \min \sum_{s=1}^S P_s [\frac{1}{T} \sum_{t=1}^T (P_{l,t,s} - \frac{1}{T} \sum_{t=1}^T P_{l,t,s})^2] \\ P_{l,t,s} = P_{l,t} - P_{w,t,s} - P_{v,t,s} \end{cases} \quad (9)$$

where  $S$  is the total number of typical wind power and PV scenarios;  $T$  is the dispatching period;  $P_s$  is the probability of occurrence of combined scenario  $S$ , %;  $P_{l,t}$  is the system load in period  $t$ , MW; and  $P_{l,t,s}$ ,  $P_{w,t,s}$  and  $P_{v,t,s}$  are the system residual load, wind power and PV output in period  $t$  of combined scenario  $s$ , MW.

The lower model reasonably arranges the output of the conventional thermal power units and CSP plants according to the system residual load curve and formulates the dispatching plan with the lowest total operation cost of the thermal power units and CSP plants. The objective function is as follows:

$$\begin{cases} f_2 = \min(F_1 + F_2 + F_3) \\ F_1 = \sum_{t=1}^T \sum_{i=1}^N [(a_i P_{it,s}^2 + b_i P_{it,s} + c_i) + u_{it}(1 - u_{i(t-1)})S_i] \\ F_2 = k_j P_{t,s}^{SF,d} + k_s P_{t,s}^{TS,df} \\ F_3 = k_i (U_{it,s} + D_{it,s}) + k_c (P_{csp,t,s}^{Up} + P_{csp,t,s}^{Down}) \end{cases} \quad (10)$$

where  $N$  is the number of thermal power units,  $N = 4$ ;  $F_1$  and  $F_2$  are the operating costs of thermal power units and the CSP plant, respectively;  $F_3$  is the system rotating reserve cost;  $a_i$ ,  $b_i$  and  $c_i$  are fuel cost coefficients of thermal power units;  $P_{it,s}$  is the generating power of thermal power unit  $i$  at time  $t$ , MW;  $u_{it}$  is the operation state of thermal power unit  $i$  at time  $t$ ,  $u_{it} = 1$  indicates unit operation,  $u_{it} = 0$  indicates unit shutdown;  $P_{t,s}^{SF,d}$  and  $P_{t,s}^{TS,df}$  are the power generation of CSP power by heat collection device and heat storage device to provide thermal energy, which can be expressed by Equations (11) and (12), respectively, MW;  $S_i$  is the startup and shutdown cost of thermal power unit  $i$ ;  $k_j$  and  $k_s$  are the operation and maintenance cost coefficients of the CSP plant by the heat collection device and by the heat storage device to provide thermal energy to generate electricity, respectively,  $k_i$  and  $k_c$  are the standby cost coefficients of thermal power units and CSP plant, respectively.

$$P_{t,s}^{SF,d} = \eta_d P_{t,s}^{SF,r} \quad (11)$$

$$P_{t,s}^{TS,df} = (1 - \eta_f) \eta_d P_{t,s}^{TS,f} \quad (12)$$

where  $\eta_d$  is the thermoelectric conversion efficiency, %;  $P_{t,s}^{SF,r}$  is the power directly generated by the collector at time  $t$ , MW;  $\eta_d$  is the is the heat release loss rate of thermal storage system, %;  $P_{t,s}^{TS,f}$  is the heat release power of the thermal storage system.

(2) Constraints

1. Power balance constraints:

$$\sum_{i=1}^N P_{it,s} + P_{w,t,s} + P_{v,t,s} + P_{csp,t,s} = P_{l,t} \tag{13}$$

where  $P_{csp,t,s}$  is the output of the CSP power station in scenario  $S$  at time  $t$ .

2. Unit output constraints

$$\left\{ \begin{array}{l} \left\{ \begin{array}{l} P_{csp\_min} \leq P_{csp,t,s} \leq P_{csp\_max}, u_{ct} = 1 \\ P_{csp,t,s} = 0, u_{ct} = 0 \end{array} \right. \\ \left\{ \begin{array}{l} P_{i\_min} \leq P_{it,s} \leq P_{i\_max}, u_{it} = 1 \\ P_{it,s} = 0, u_{it} = 0 \end{array} \right. \\ 0 \leq P_{w,t,s} \leq P_{wind\_max} \\ 0 \leq P_{v,t,s} \leq P_{v\_max} \end{array} \right. \tag{14}$$

where  $P_{csp\_min}$ ,  $P_{csp\_max}$  are the upper and lower limits of the output of the CSP power station;  $u_{ct}$  is the operation state of CSP plant at time  $t$ ,  $u_{ct} = 1$  indicates unit operation,  $u_{ct} = 0$  indicates unit shutdown;  $P_{i\_min}$ ,  $P_{i\_max}$  are the upper and lower limits of the output of the thermal power unit, respectively;  $P_{wind\_max}$ ,  $P_{v\_max}$  are the upper and lower limits of the output of the wind and solar power plant.

3. Unit rotating reserve constraints:

$$\left\{ \begin{array}{l} U_{i,t,s} = \sum_{i=1}^N (P_{i\_max} - P_{it,s}, r_{ui}) \geq P_{c,t,s} \\ D_{i,t,s} = \sum_{i=1}^N (P_{it,s} - P_{i\_min}, r_{di}) \geq P_{c,t,s} \\ P_{csp,t,s}^{Up} \leq P_{csp\_max} - P_{csp,t,s} \\ P_{csp,t,s}^{Down} \leq P_{csp,t,s} - P_{csp\_min} \end{array} \right. \tag{15}$$

where  $U_{i,t,s}$ ,  $D_{i,t,s}$ ,  $P_{csp,t,s}^{Up}$  and  $P_{csp,t,s}^{Down}$  are the positive and negative rotating reserve capacities of the thermal power units and CSP plant, respectively;  $P_{c,t,s}$  is the prediction error of the system load; and  $P_{c,t,s} = P_{l,t,s}L$ ,  $L$  is the error rate of load forecasting.

4. Ramp rate constraints:

$$\left\{ \begin{array}{l} -r_{di} \leq P_{it,s} - P_{i(t-1),s} \leq r_{ui} \\ -r_{d\_csp} \leq P_{csp,t,s} - P_{csp,(t-1),s} \leq r_{u\_csp} \end{array} \right. \tag{16}$$

where  $r_{di}$  and  $r_{ui}$  are the maximum up and down ramp rates of thermal power unit  $i$ , respectively, and  $r_{d\_csp}$  and  $r_{u\_csp}$  are the maximum up and down ramp rates of the CSP power plant, respectively.

### 5. Thermal storage system constraints:

$$E_{h,t,s} = (1 - \tau)E_{h,t-1,s} - \frac{P_{t,s}^{\text{TS},f}}{\eta_f} + \eta_c P_{t,s}^{\text{TS},c} \quad (17)$$

$$\begin{cases} E_{h\_min} \leq E_{h,t,s} \leq E_{h\_max} \\ P_{min}^{\text{TS},c} \leq P_{t,s}^{\text{TS},c} \leq P_{max}^{\text{TS},c} \\ P_{min}^{\text{TS},f} \leq P_{t,s}^{\text{TS},f} \leq P_{max}^{\text{TS},f} \\ P_{t,s}^{\text{TS},c} P_{t,s}^{\text{TS},f} = 0 \end{cases} \quad (18)$$

where  $E_{h,t,s}$  is the heat storage capacity of the thermal storage system at time  $t$ , MW·h;  $E_{h\_min}$  and  $E_{h\_max}$  are the minimum and maximum heat storage capacity of the thermal storage system of the CSP plant;  $P_{min}^{\text{TS},c}$  and  $P_{min}^{\text{TS},f}$  are the minimum heat charging and discharging power of the thermal storage system at time  $t$ , respectively;  $P_{max}^{\text{TS},c}$  and  $P_{max}^{\text{TS},f}$  are the maximum heat charging and discharging power of the thermal storage system at time  $t$ , respectively;  $\tau$  is the heat loss coefficient of the thermal storage system.

### 3.2. Intraday Scheduling Plan Model

#### (1) Objective function

The intraday rolling model is divided into two layers. The upper model takes the minimum expected value of the system residual load variance as the objective function, and the lower model takes the minimum total operation cost of thermal power units and CSP plants as the objective function:

$$\begin{cases} f_3 = \min[\frac{1}{T} \sum_{t=1}^T (P_{l,t} - \frac{1}{T} \sum_{t=1}^T P_{l,t})^2] \\ P_{l,t} = \tilde{P}_{l,t} - \tilde{P}_{w,t} - \tilde{P}_{v,t} \end{cases} \quad (19)$$

where  $\tilde{P}_{l,t}$  is the intraday load demand fuzzy number;  $\tilde{P}_{w,t}$  is the intraday wind power output fuzzy number; and  $\tilde{P}_{v,t}$  is the intraday PV output fuzzy number.

$$\begin{cases} f_4 = \min(F_5 + F_6 + F_7) \\ F_5 = \sum_{t=1}^T \sum_{i=1}^N [(a_i P_{it}^2 + b_i P_{it} + c_i)] \\ F_6 = k_j P_t^{\text{SF},d} + k_{\text{TS}} P_t^{\text{TS},df} \\ F_7 = k_i (U_{it} + D_{it}) + k_c (P_{\text{csp}_t}^{\text{Up}} + P_{\text{csp}_t}^{\text{Down}}) \end{cases} \quad (20)$$

where  $F_5$  is the operating cost of the thermal units. Since the start/stop status of the thermal units is determined in the day-ahead dispatch, only fuel cost is considered in the intraday dispatch.

#### (2) Constraints

##### 1. Power balance constraints:

$$Cr \left\{ \sum_{t=1}^T \sum_{i=1}^N P_{it} + \tilde{P}_{w,t} + \tilde{P}_{v,t} + P_{\text{csp}_t} = \tilde{P}_{l,t} \right\} \geq \alpha \quad (21)$$

where  $\alpha$  is the confidence level.

## 2. Units spinning reserve constraints:

$$\begin{cases} Cr \left\{ \sum_{t=1}^T \sum_{i=1}^N U_{i,t} + \sum_{t=1}^T P_{csp,t}^{Up} \geq L\tilde{P}_{l,t} \right\} \geq \alpha \\ Cr \left\{ \sum_{t=1}^T \sum_{i=1}^N D_{i,t} + \sum_{t=1}^T P_{csp,t}^{Down} \leq L\tilde{P}_{l,t} \right\} \geq \alpha \end{cases} \quad (22)$$

In this paper, the constraints of CSP plant heat storage capacity, thermal energy storage (TES) heat storage and release power, and that heat storage and release cannot be carried out at the same time in the same period, are referred to in [19].

### 3.3. Scenario Generation and Reduction

The mean and variance of the wind and PV prediction errors are obtained using data processing of the actual and predicted output of the original wind and PV of the system. Figures 2 and 3 show the 30-day forecast errors of wind power and PV, respectively. For the forecast errors of wind and PV at 24 time points in each day, assuming that the probability of occurrence at each time point is the same, the data exceeding the upper and lower limits of the forecast error will be discarded, and the expectation and variance of the forecast errors of wind and PV can be obtained by using the 30-day data:  $\mu_{w,t,c} = 0.012$ ,  $\mu_{v,t,c} = 0.008$ ,  $\delta_{w,t,c} = 1.003$ ,  $\delta_{v,t,c} = 1.001$ . Therefore, the wind power output prediction error approximately obeys the standard normal distribution.

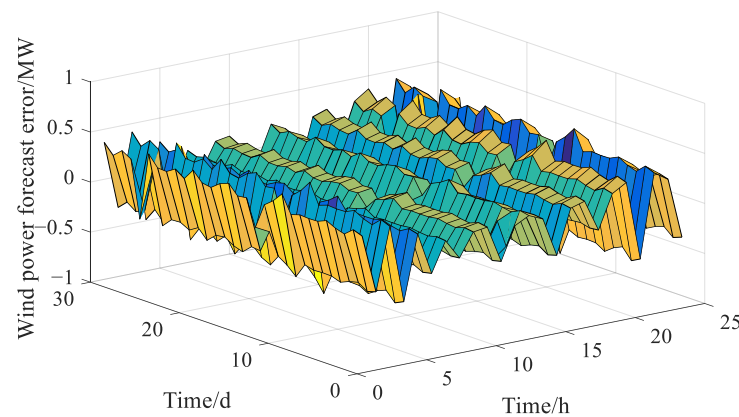


Figure 2. Wind power prediction error.

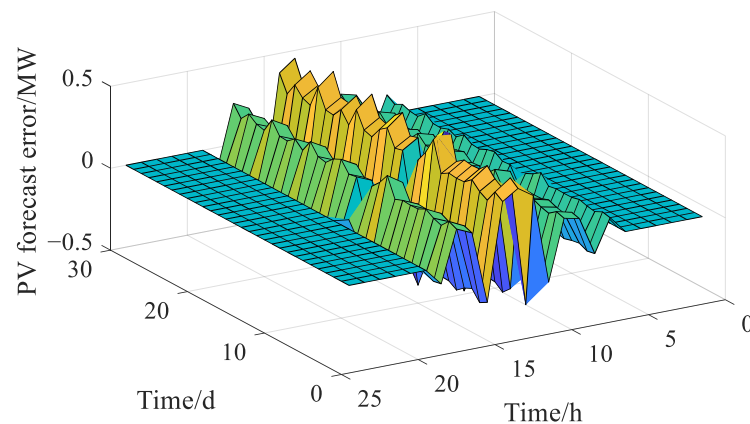


Figure 3. PV power prediction error.

### 3.4. Day-Ahead Multiscene Stochastic Programming Model

In day-ahead scheduling, the determined scenario set is used to characterize the uncertainty of the day-ahead new energy output.

(1) Scenario generation

By analyzing the prediction errors of wind power and PV, Latin hypercube sampling (LHS) is used to sample its probability distribution, and 120 wind power and PV scene sets are randomly generated. Through preliminary analysis and comparison, 100 scenes with large prediction errors are retained after deletion. LHS belongs to stratified sampling, which reflects the overall distribution of random variables by using the sampling values. Its essence is to forcibly extract the points in each layer by layering the input probability distribution to ensure that the sampling points can cover all the sampling areas. The sampling diagram is shown in Figure 4.

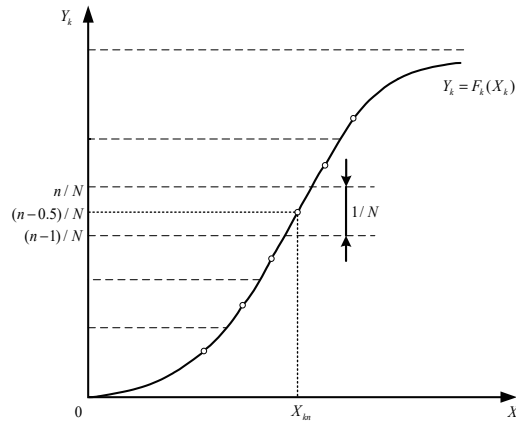


Figure 4. Latin hypercube sampling (LHS) schematic.

Assuming that  $X_k (k = 1, 2, 3 \dots k)$  is  $k$  a random variable of  $K$  problems to be solved, its cumulative probability distribution function can be expressed as:

$$Y_k = F_k(X_k) \tag{23}$$

Assuming that the total number of samples is  $N$ , on the interval  $[0,1]$ , the longitudinal axis of  $Y_k = F_k(X_k)$  is divided into  $N$  intervals by LHS. The intervals are equal, the width of the intervals is  $1/N$ , and each interval is independent of each of the others.  $Y_k$  is the sampling value at the midpoint of each interval,  $X_k$  is its corresponding abscissa, and the calculation formula of the  $n$  sampling value of  $X_k$  is as follows:

$$X_{kn} = F_k^{-1}\left(\frac{n - 0.5}{N}\right) \tag{24}$$

When all the random variables are sampled, an initial sampling matrix of  $N \times N$  order is obtained. Figures 5 and 6 show the obtained set of initial sampling scenarios for wind and PV.

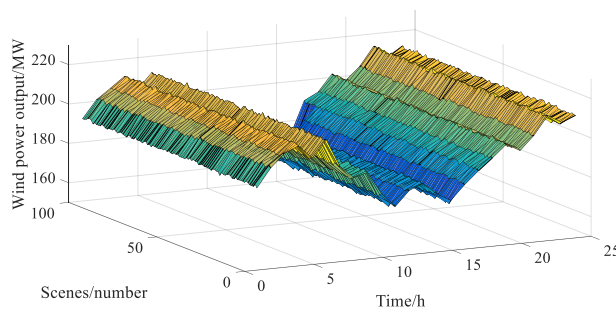
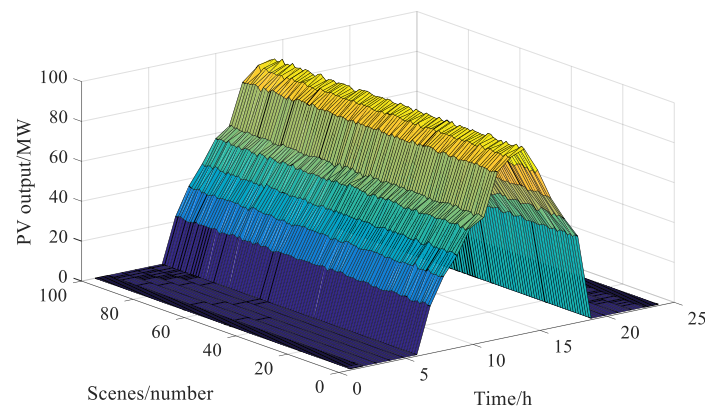


Figure 5. Wind power output scenario.



**Figure 6.** PV power output scenario.

## (2) Scenario reduction

Large-scale scenes will increase the amount of computation, and the purpose of scene reduction is to replace numerous generated scenes with a small number of typical scenes. Therefore, a set of “clustered” and representative typical scenes can be obtained by clustering technology. In this paper, the synchronous back substitution elimination method is used to reduce a large number of scenes. The specific reduction steps are as follows:

Step 1: For scene  $\lambda_i$  ( $i = 1, 2, \dots, L$ ), calculate scene  $\lambda_j$  with the shortest distance.

$$D_{i,\min} = \min_j \delta_j d(\lambda_i, \lambda_j) \quad (25)$$

where  $\delta_j$  is the probability of occurrence of scenario  $\lambda_j$  and  $d(\lambda_i, \lambda_j)$  is the Euclidean distance between two scenarios.

Step 2: Determine the scene to be deleted.

$$D_{\min} = \min_{i=1,2,\dots,L} \delta_i D_{i,\min} \quad (26)$$

Step 3: modify the number of remaining scenes  $L = L - 1$ , add the probability of deleted scenes to the nearest scene and ensure that the sum of the probabilities of all scenes is 1.

Step 4: Repeat Steps 1–3 until the number of remaining scenes reaches the desired set value  $m$ .

Figure 7 shows the typical wind and PV output scenarios after scenario reduction, with three wind and PV output scenarios reserved.

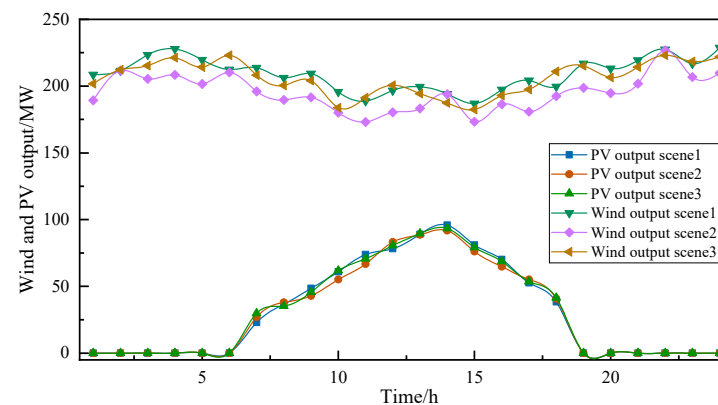


**Figure 7.** Typical wind and PV output scenarios.

### (3) Scenario combination

Based on the assumption that all kinds of new energy output are independent of each other, the typical scenes of wind power and PV output after reduction are combined by a Cartesian product. The total number of combined scenes and the probability of corresponding scenes are:

$$\begin{cases} N_s = N_w * N_v \\ P_{i,j} = P_i * P_j \end{cases} \quad (27)$$

In the formula,  $N_s$  is the total number of composite scenarios;  $N_w$  and  $N_v$  are the number of typical scenarios of wind power and PV output, respectively;  $P_{i,j}$  is the probability of occurrence of combined scenarios; and  $P_i$  and  $P_j$  are the probability of typical scenarios of wind power and PV output, respectively.

### 3.5. Model Solving

In this paper, the upper-level optimal dispatching model uses the renewable energy output forecast data for rolling optimization, with the minimum expected value of the residual load variance as the objective function. The lower-level economic optimal dispatch model contains two types of decision variables: 0–1 variables and integer variables, so the solved model is a typical mixed-integer programming model, which can be solved by using mixed-integer programming or commercial software. The calculation flow chart of the bilevel optimization model is shown in Figure 8.

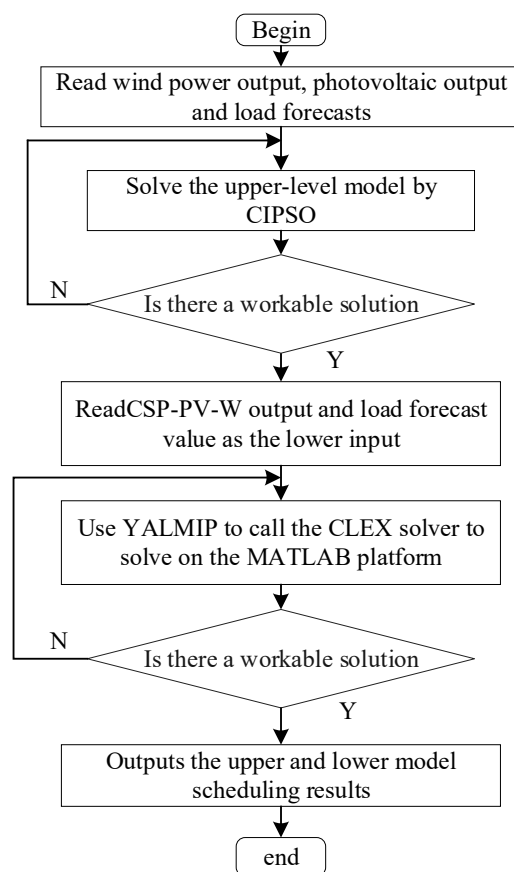


**Figure 8.** Flow chart of two-level optimization.

The calculation example in this paper uses a computer platform with Intel Core I5-5200U and 16 GB of running memory, which calls the commercial optimization software CPLEX through YALMIP to solve it, and solves it through the solution process shown in Figure 8. The algorithm architecture adopted by CPLEX solver to solve mixed-integer

programming (MIP) problems is Branch-and-Cut, and heuristic algorithms are applied at the root node and other nodes to improve the efficiency of solution. The calculation time of each instance of the model is between 20 s and 240 s.

#### 4. Example Analysis

According to the day-ahead scheduling results, the output plans of each unit in nine typical scenarios are obtained. The consumption rates of wind power and PV in each scenario are 93.75% and 92.62%, respectively, and the total expected operating cost of the system in each scenario is CNY 70.011 million. Intraday scheduling analyzes the output plans of each unit, wind power PV consumption rate and comprehensive operating cost under different confidence levels, and compares it with the day-ahead scheduling plan. The results show that for new power systems with uncertain source loads, intraday short time scale scheduling is more economical than day-ahead long time scale scheduling. Compared with the scheduling model in literature [20], the multi-timescale scheduling model proposed in this paper has a higher wind power and PV power consumption rate under the same optimization objective.

##### 4.1. Model Solving

This example includes four thermal power units with an installed capacity of 255 MW, a 100 MW CSP plant, a wind power installed capacity of 280 MW participating in system dispatching, and a PV installed capacity of 100 MW. The specific operating parameters of the thermal power units and CSP plant are shown in Appendix A Tables A1 and A2. The operation and maintenance cost coefficients of the CSP plant are  $k_j = 20$  yuan/MW and  $k_s = 30$  yuan/MW, respectively. The rotating reserve cost coefficients of the thermal power units and CSP power plants are 120 yuan/MW and 50 yuan/MW, respectively.

##### 4.2. Analysis of Example Results

###### 4.2.1. Analysis of Day-Ahead Results

Figure 9 shows the dispatching output of thermal power units in different scenarios. Figure 10 shows the dispatching output of the CSP plant, and Figure 11 shows the dispatching output of wind power and PV.

Combined with the analysis in Figures 9–11, it can be determined that the PV output is almost zero at 1–6 h and 18–24 h. Due to the limitation of the system heat storage capacity, the output of the CSP plant is also relatively reduced. In this period, the output of thermal power units is significantly increased, especially at 18–22 h, in the peak load period, and the thermal power units are almost allowed to operate at the maximum output level. From 7 to 17 h, the overall output of new energy sources increases significantly, which reduces the system operation cost while relieving the pressure on thermal units. At the same time, during 1–6 h and 18–24 h, which is also the time of wind power generation, the output of the CSP plant can be reduced appropriately to make room to allow wind power to be connected to the grid by taking advantage of its flexible and controllable characteristics.

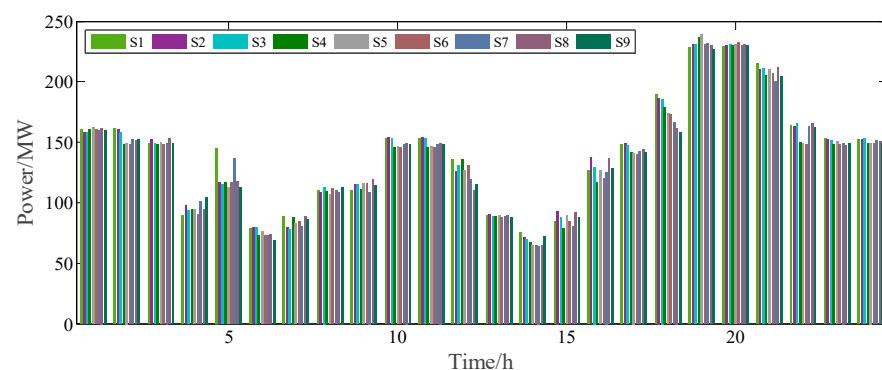


Figure 9. Scheduling output of the thermal power units.

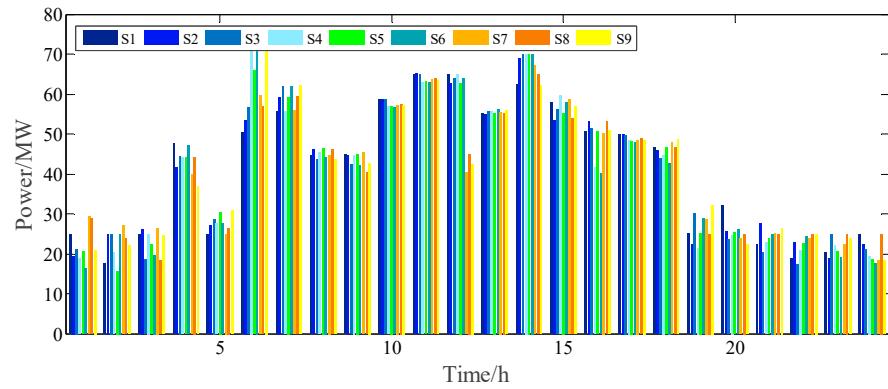


Figure 10. Scheduling output of the CSP plant.

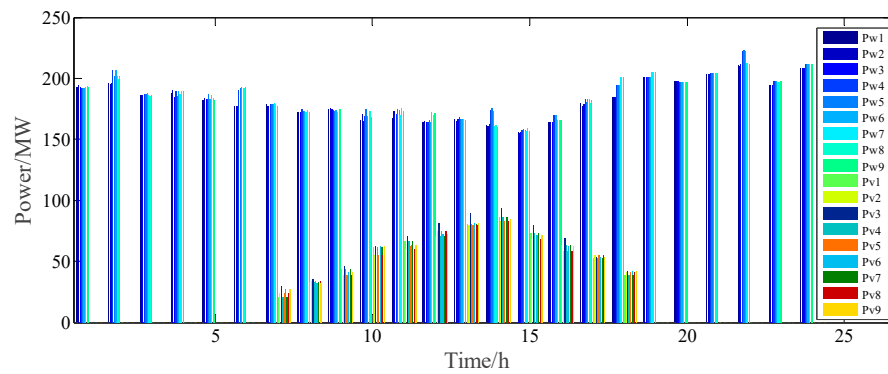


Figure 11. Wind power and PV scheduling output.

Figure 12 shows the heat storage state of the CSP plant in the combined scenario. At 1–7 h and 18–24 h, due to the absence of solar illumination, the CSP plant has almost no output. The heat storage system releases the stored heat to promote the power generation of the turbine unit and increase the output of the CSP plant, thereby reducing the output of the thermal power units. At 8–17 h, the solar illumination is strong, and the CSP plant cooperates with the thermal power units to participate in the peak shaving of the system. At the same time, part of the heat is stored in the heat storage device to prepare for the continuous output of the CSP plant without solar illumination at night.

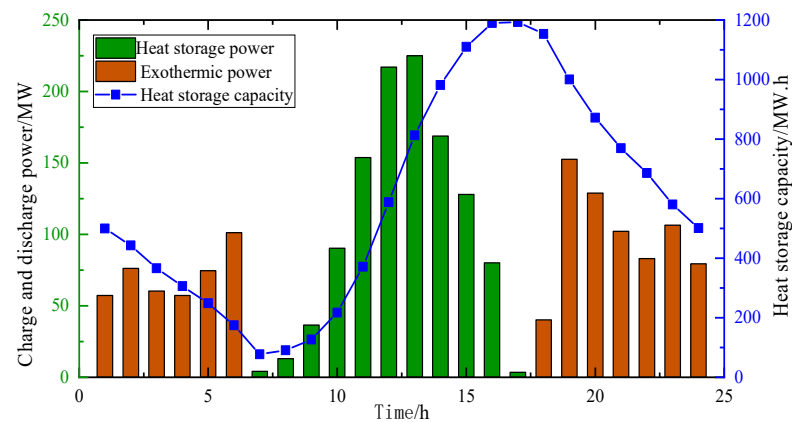


Figure 12. Status of the thermal storage system of the solar thermal power plant.

Table 1 shows that among the nine scenarios, the PV consumption rate in scenario 2 reaches the maximum, while the maximum consumption rate of wind power appears in scenario 8. Therefore, separate scheduling for each scenario cannot achieve the most ideal results. The PV consumption rate of each scenario is multiplied by the scenario combination

probability to obtain a wind power consumption rate of 93.75% and a PV consumption rate of 92.62%. Although the comprehensive utilization rate of wind and PV has not reached the maximum, Table 2 shows that the comprehensive operating cost of the scene system with high wind and PV absorption rates is also high.

**Table 1.** Wind and PV absorption rates in different scenes.

Scenarios	Combined Scene Probability %	Wind Power Consumption Rate %	PV Power Consumption Rate %
S1	11.25	94.0	91.2
S2	7.5	94.6	97.6
S3	6.25	93.8	94.3
S4	15.75	94.1	92.3
S5	10.5	93.9	92.8
S6	8.75	94.5	93.1
S7	18	92.6	92.3
S8	12	95.3	91.8
S9	10	93.9	90.9

In each scenario, the wind power consumption rate is 93.75%, and the PV consumption rate is 92.62%.

**Table 2.** Expected operating costs of the system in different scenarios.

Scenarios	Comprehensive Cost/Million Yuan	Combined Scene Probability %	Comprehensive Cost after Multiplying Probability Million Yuan
S1	70.561	11.25	7.938
S2	70.916	7.5	5.318
S3	71.618	6.25	4.476
S4	69.402	15.75	10.93
S5	69.807	10.5	7.329
S6	69.618	8.75	6.091
S7	69.887	18	12.579
S8	69.572	12	8.348
S9	69.971	10	6.997

The total expected operating cost of the system in each scenario is CNY 70.011/million.

#### 4.2.2. Analysis of Intraday Results

Figure 13 shows the dispatching output of four thermal power units at different confidence levels.

Combined with the analysis in Figure 13, we can conclude that during the 70–90 period of load peak, the four thermal power units, G1, G2, G3 and G4, maintain full-load operation. In the period of 15–30 with low load, the wind power generation is large in this period. The output of the G3 and G4 thermal power units is lower than the minimum level of their economic operation, so they are shut down in this period. During the shutdowns of G3 and G4, the output of G1 and G2 increased slightly but not much, both in the economical operating range.

Figure 14 shows the dispatched output of the CSP plant, the dispatched output of wind power and PV, and the upper rotating reserve capacity of the thermal units and CSP plant at different confidence levels.

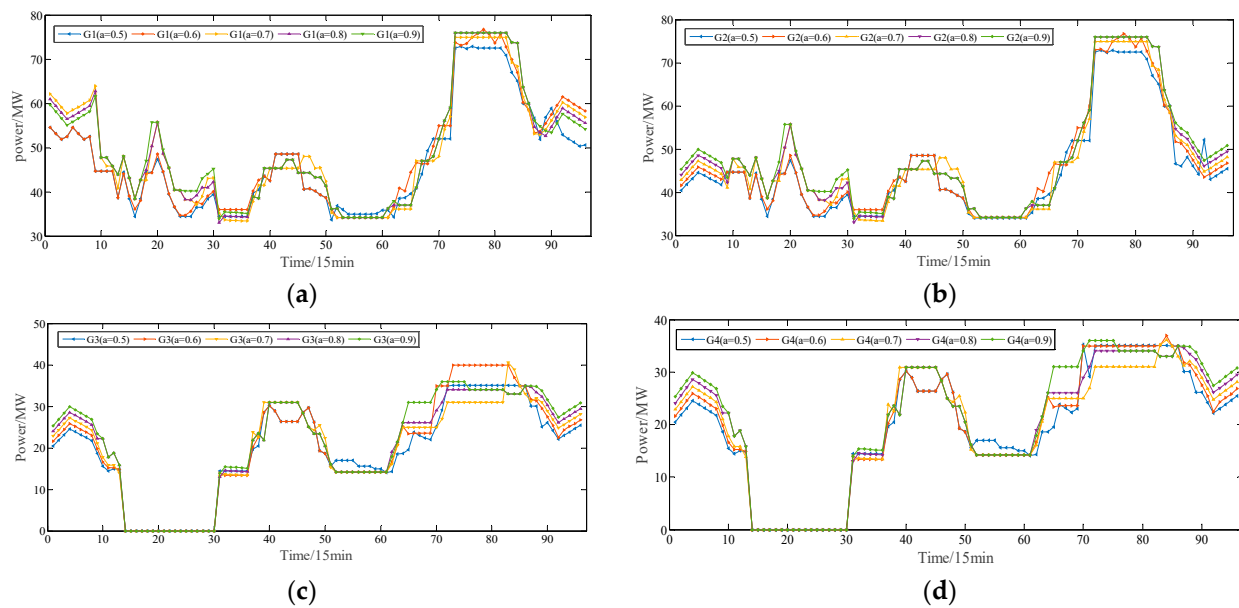


**Figure 13.** Scheduling output of four thermal power units at different confidence levels. (a) G1 output at different confidence levels; (b) G2 output at different confidence levels; (c) G3 output at different confidence levels; (d) G4 output at different confidence levels.

Figure 14a shows that while the output of the CSP plant is fully consumed, the output adjustment of the CSP plant increases with the increasing confidence level. When the confidence level is 0.5, the output of the CSP plant accounts for 36.52% of the total output in the 35–50 and 70–90 periods, while the confidence level is 0.9, accounting for 41.19%. Similarly, according to Figure 14b, the consumption of wind power and PV also increases with the increasing confidence level. According to Figure 14c, the reserve capacity of the system also increases with the increasing confidence level. Compared with the reserve capacity of the CSP plant and thermal power units when the confidence level is 0.5 and 0.9, the reserve capacity increases by 6.03% and 5.95%, respectively.

Figures 15 and 16 show the comparison of the wind power and PV consumption rate and total system operation cost at different confidence levels in the intraday dispatch and the wind power and PV consumption rate and total system operation cost at the combined field in the day-ahead dispatch.

Figure 15 shows that in the intraday scheduling model, the consumption rates of wind power and PV power gradually increase with the increasing confidence level. Under different confidence levels, the PV consumption rate of intraday scheduling is always higher than the PV consumption rate of day-ahead scheduling. The wind power consumption rate of intraday scheduling is higher than the wind power consumption rate of day-ahead scheduling only when the confidence level is greater than 0.8. However, combined with Figure 16, with the increase in confidence level, the total operating cost of the system also increases while the new energy consumption increases. Figure 15 shows that when the confidence level is 0.5, 0.6 and 0.7, the total cost of the intraday scheduling system is 4.86%, 4.551% and 0.428% lower than that of day-ahead scheduling, respectively. Once the confidence level exceeds 0.7, the total cost of the intraday scheduling must be greater than that of the day-ahead scheduling.

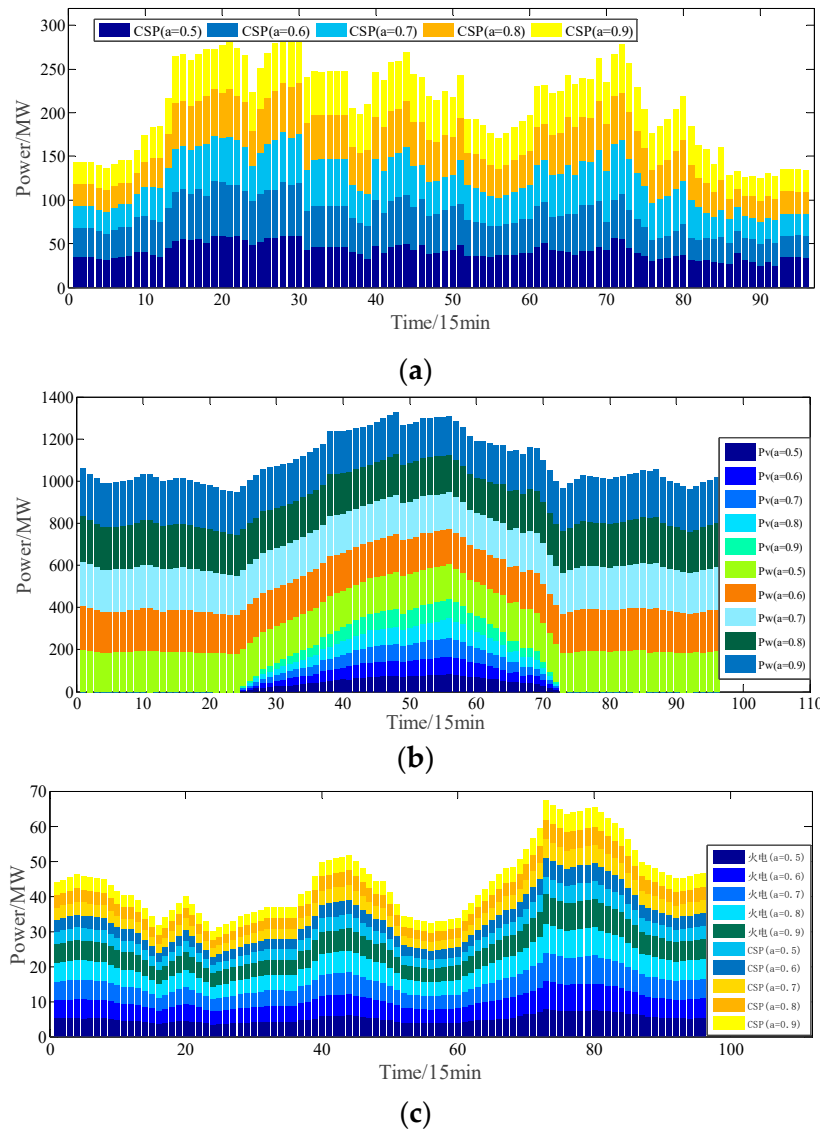


**Figure 14.** Output of each power and rotating reserve capacity at different confidence levels. (a) Output of CSP plant at different confidence levels. (b) Output of wind power and PV at different confidence levels. (c) Upper rotating reserve capacity of the thermal units and CSP plant at different confidence levels.

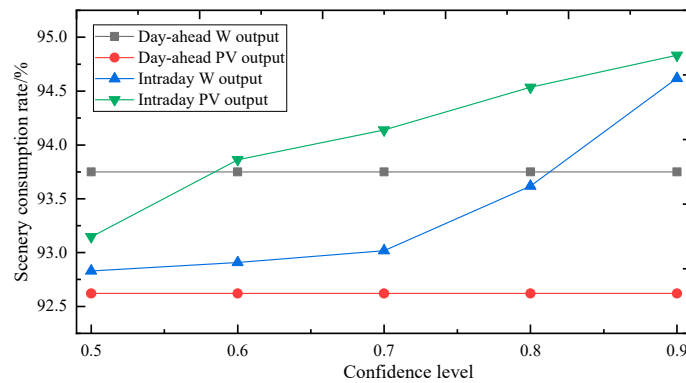


**Figure 15.** Consumption rate of wind power and PV power at different confidence levels.

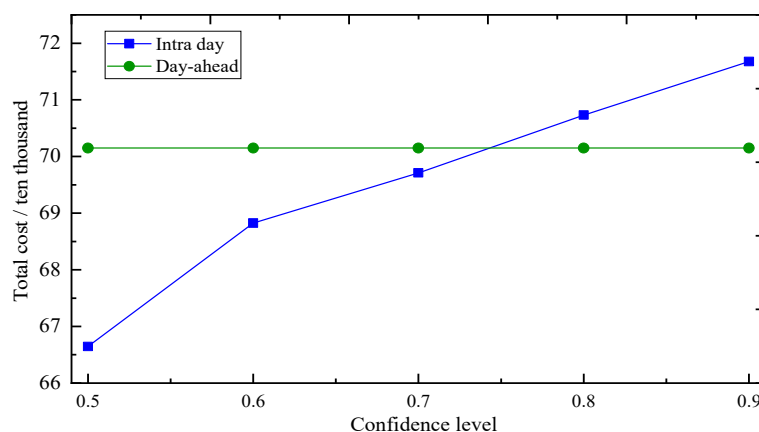


**Figure 16.** Total system operation cost at different confidence levels.

Table 3 shows that if the confidence level is 0.5 is the base value, with the increase in confidence level, the comprehensive operating cost of the system increases by 3.1%, 4.39%, 6.13%, and 7.54%, respectively. The reserve cost of thermal power units increases by 2.34%, 3.04%, 4.34% and 5.62%, respectively. The reserve cost of the CSP plant increases by 2.33%, 4.16%, 5.43% and 5.63%, respectively. It can be found that when the confidence degree of the intraday scheduling plan is less than or equal to 0.8, the comprehensive operating cost of the system is always lower than the expected operating cost of the system in each scenario before the day. Therefore, for the system with source load uncertainty, the intraday short time scale scheduling plan is more economical than the long-timescale ahead of the day. With the lowest comprehensive operation cost as the optimization objective, the wind power and PV power consumption rates of the model proposed in this paper are lower than the operation results of the scheduling model proposed in the literature [20] at all confidence levels: 92.19%.

**Table 3.** System operation cost at different confidence levels.

Confidence Level	Comprehensive Operation Cost Million Yuan	Wind Power Consumption Rate %	PV Power Consumption Rate %
a = 0.5	66.646	92.83	93.14
a = 0.6	68.825	92.92	93.86
a = 0.7	69.711	93.01	94.14
a = 0.8	70.732	93.61	94.53
a = 0.9	71.676	94.66	94.86

## 5. Conclusions

Aiming to solve the problem regarding the efficient accommodation of a large-scale wind-solar grid-connected system, a day-ahead and intraday coordinated optimal scheduling strategy considering the uncertainty of the source and load is proposed in this paper. The objective is to minimize the expected value of the residual load variance and the operating cost of the system. The following conclusions are obtained by numerical example analysis:

- (1) A multi-scenario analysis method is used to convert the uncertainty of the day-ahead forecast output of wind and solar energy into a deterministic scenario, and then the fuzzy theory is introduced. The trapezoidal fuzzy number equivalent model is used to characterize the uncertainty of the day-ahead wind and solar energy and load. The example shows that the model can effectively alleviate the problem of a high proportion of new energy-efficient consumption caused by prediction error and wind and solar output fluctuation.

- (2) Multiperiod coordinated scheduling can combine more accurate intraday prediction information and make full use of the fast adjustment ability and power shift characteristics of the CSP plants, which can effectively reduce the fluctuation of load after the wind–solar grid connection, thereby reducing the comprehensive operation cost of the system.

This paper aims to propose a feasible scheme for the current dilemma of power system peak regulation, which has a certain reference value for the CSP plant to participate in power market dispatching. The multi-scenario stochastic planning method, through the historical data of wind and solar output, is appropriate to generate the wind power probability distribution model, which is based on the probability distribution model for sampling, to generate different scenarios. Since a large number of scenarios will increase the complexity of the optimization target solution, the scenario reduction is required. At the same time, the scenario reduction cannot cover all the possible scenarios that decision makers need to consider. The CSP plant is limited by light resources and heat storage capacity, resulting in limited peak regulation capacity. The size of the backup capacity on the source side of the flexible adjustment directly affects the curtailment rate of new energy and the operating cost of the system. However, due to the scheduling constraints such as the adjustment period and the uncertainty of new energy output, the uncertainty of only one side will gradually weaken the improvement effect. Therefore, the uncertainty on both sides of the source and load can be fully considered to maximize the economic capacity of the system.

**Author Contributions:** Conceptualization, M.X. and Z.W.; Methodology, W.L.; Validation, W.L., Z.F. and W.B.; Formal analysis, Z.F.; Investigation, L.J. and Z.W.; Data curation, L.J.; Writing—original draft, L.J.; Writing—review & editing, Z.W.; Visualization, W.B.; Supervision, M.X.; Project administration, W.L.; Funding acquisition, M.X. All authors have read and agreed to the published version of the manuscript.

**Funding:** This research was funded by Gansu Province Electric Power Company Cooperation Project grant number SGGJY00GHYBWT2200015 and the APC was funded by Gansu Province Electric Power Company Cooperation Project.

**Data Availability Statement:** The data that support the findings of this study are available from the corresponding author upon reasonable request.

**Conflicts of Interest:** The authors declare no conflict of interest.

## Appendix A

**Table A1.** Operation parameters of thermal power units.

Unit	Upper Limit of Output (MW)	Lower Limit of Output (MW)	Ramp Rate (MW/h)	Fuel Cost			Start-Up and Shut-Down Costs
				a Yuan/MW	b Yuan/MW	c Yuan/MW	H Yuan/MW
1	80	40	40	0.02	179	295	1456
2	80	40	40	0.031	175	350	1729
3	50	20	20	0.023	100	125	1982
4	50	20	20	0.015	125	167	2464

**Table A2.** Operation parameters of the CSP plant.

Operation Parameters of CSP Plant	Value
Rated output power of CSP plant/MW	100
Minimum output power during operation of CSP plant/MW	10
Maximum ramp rate of CSP plant/MW/h	40
Heat loss rate of heat storage system/%	3
Thermoelectric conversion efficiency of CSP plant/%	45
Photothermal conversion efficiency of CSP plant/%	57
Cost coefficient of heating and power generation for collectors/(yuan/MW·h)	20
Cost coefficient of power generation for heat storage devices/(yuan/MW·h)	40
Maximum daily heat storage capacity of heat storage system/MW·h	1000
Initial value of heat storage capacity of heat storage system/MW·h	600
The lower limit of heat storage system/MW·h	100
Mirror field area/m	$1.33 \times 106$
Dissipation coefficient of heat storage system/%	3.1
Heat storage efficiency of heat storage system/%	98.5
Heat release efficiency of heat storage system/%	98.5

## References

- Zhang, X.; Zhao, C.; Liang, J.; Li, K.; Zhong, J. Robust fuzzy scheduling of power systems considering bilateral uncertainties of generation and demand side. *Autom. Electr. Power Syst.* **2018**, *42*, 67–75. [[CrossRef](#)]
- Wang, H.; Qin, H.; Zhou, C.; Jia, F.; Xu, X.; Pan, X. Cross-regional day-ahead to intra-day scheduling model considering forecasting uncertainty of renewable energy. *Autom. Electr. Power Syst.* **2019**, *43*, 60–67.
- Jin, H.; Sun, H.; Niu, T.; Guo, Q. Robust unit commitment considering uncertainties of wind and energy intensive load dispatching. *Autom. Electr. Power Syst.* **2019**, *43*, 13–20. [[CrossRef](#)]
- Zhang, J.; Cheng, C.; Shen, J.; Li, G.; Li, X. Short-term Joint Optimal Operation Method for High Proportion Renewable Energy Grid Considering Wind-solar Uncertainty. *Proc. Chin. Soc. Elec. Eng.* **2020**, *40*, 5921–5932. [[CrossRef](#)]
- Yuan, Q.; Wu, Y.; Li, B.; Sun, Y.; Lai, X.; Zhong, H. Multi-timescale coordinated dispatch model and approach considering generation and load uncertainty. *Power Syst. Prot. Control* **2019**, *47*, 8–16.
- Wang, Q.; Wang, J.; Guan, Y. Stochastic unit commitment with uncertain demand response. *IEEE Trans. Power Syst.* **2013**, *28*, 562–563. [[CrossRef](#)]
- Zhao, C.; Wang, J.; Watson, J.P.; Guan, Y. Multi-stage robust unit commitment considering wind and demand response uncertainties. *IEEE Trans. Power Syst.* **2012**, *28*, 2708–2717. [[CrossRef](#)]
- Yang, S.; Zeng, D.; Ding, H.; Yao, J.; Wang, K. Multi-objective demand response model considering the probabilistic characteristic of price elastic load. *Energies* **2016**, *9*, 80. [[CrossRef](#)]
- Jin, G.; Pan, D.; Chen, Q.; Shi, C.; Li, G. Fuzzy random day-ahead optimal dispatch of dc distribution network considering the uncertainty of source-load. *Trans. Chin. Electrotechn. Soc.* **2021**, *36*, 4517–4528. [[CrossRef](#)]
- Ma, R.; Kang, R.; Jiang, F.; Xiong, L.; Li, L.; Xu, H. Multi-objective dispatch planning of power system considering the stochastic and fuzzy wind power. *Power Syst. Prot. Control* **2013**, *41*, 150–156.
- Cui, Y.; Li, C.; Zhao, Y.; Zhong, W.; Wang, M. Source-grid-load multi-time interval optimization scheduling method considering wind-photovoltaic-photothermal combined DC transmission. *Proc. Chin. Soc. Elec. Eng.* **2022**, *42*, 559–573. [[CrossRef](#)]
- Xiong, H.; Xiang, T.; Chen, H.; Lin, F.; Su, J. Research of fuzzy chance constrained unit commitment containing large-scale intermittent power. *Proc. Chin. Soc. for Elec. Eng.* **2013**, *33*, 36–44. [[CrossRef](#)]
- Zhao, D.; Yin, J. Fuzzy random chance constrained preemptive goal programming scheduling model considering source-side and load-side uncertainty. *Trans. Chin. Electrotech. Soc.* **2018**, *33*, 1076–1185. [[CrossRef](#)]
- Li, W.; Zhou, J.; Xie, K.; Xiong, X. Power system risk assessment using a hybrid method of fuzzy set and Monte Carlo simulation. *IEEE Trans. Power Syst.* **2008**, *23*, 336–343. [[CrossRef](#)]
- Li, G.; Li, X.; Bian, J.; Li, Z. Two level scheduling strategy for inter-provincial dc power grid considering the uncertainty of PV-load prediction. *Proc. Chin. Soc. Elec. Eng.* **2021**, *41*, 4763–4776. [[CrossRef](#)]
- Zhong, W.; Huang, S.; Cui, Y.; Xu, J.; Zhao, Y. W-S-C Capture coordination in virtual power plant considering source-load uncertainty. *Power Syst. Technol.* **2020**, *44*, 3424–3432. [[CrossRef](#)]
- Jiang, Z.; Li, S.; Ma, X.; Li, X.; Kang, Y.; Li, H.; Dong, H. State estimation of regional power systems with source-load two-terminal uncertainties. *Comp. Model. Eng.* **2022**, *132*, 295–317. [[CrossRef](#)]
- Li, Z.; Zhang, Z. Day-ahead and intra-day optimal scheduling of integrated energy system considering uncertainty of source & load power forecasting. *Energies* **2021**, *14*, 2539. [[CrossRef](#)]

19. Chen, R.; Sun, H.; Li, Z.; Liu, Y. Grid dispatch model and interconnection benefit analysis of concentrating solar power plants with thermal storage. *Autom. Electr. Power Syst.* **2014**, *38*, 1–7. [[CrossRef](#)]
20. Cui, Y.; Yang, Z.; Zhang, J.; Wang, M.; Yan, G. Scheduling strategy of wind power-photovoltaic power-concentrating solar power considering comprehensive costs. *High Vol. Eng.* **2019**, *45*, 269–275.

**Disclaimer/Publisher’s Note:** The statements, opinions and data contained in all publications are solely those of the individual author(s) and contributor(s) and not of MDPI and/or the editor(s). MDPI and/or the editor(s) disclaim responsibility for any injury to people or property resulting from any ideas, methods, instructions or products referred to in the content.